3D simulation of H-mode plasmas with localized divertor impurity injection on Alcator C-Mod using the 3D edge transport code EMC3-EIRENE[a)]

J.D. Lore[1,b)], M.L. Reinke[2], D. Brunner[3], B. LaBombard[3], B. Lipschultz[2], J. Terry[3], R.A. Pitts[4], Y. Feng[5]

[1]*Oak Ridge National Laboratory, Oak Ridge TN, 37831, USA*

[2]*York Plasma Institute, Department of Physics, University of York, Heslington, York YO10 5DD, UK*

[3]*Plasma Science and Fusion Center, MIT, Cambridge, MA 02139, USA*

[4]*ITER Organization, Route de Vinon-sur-Verdon, CS 90046 - 13067 Saint Paul Lez Durance Cedex, France*

[5]*Max Planck Institute for Plasma Physics, Greifswald Germany*

I. Abstract

Experiments in Alcator C-Mod to assess the level of toroidal asymmetry in divertor conditions resulting from poloidally and toroidally localized extrinsic impurity gas seeding show a weak toroidal peaking (~1.1) in divertor electron temperatures for high-power Enhanced D-alpha H-mode plasmas. This is in contrast to similar experiments in Ohmically heated L-mode plasmas, which showed a clear toroidal modulation in the divertor electron temperature. Modeling of these experiments using the 3D edge transport code EMC3-EIRENE [Y. Feng, et al., J. Nucl. Mater., 241 (1997) 930] qualitatively reproduces these trends, and indicates that the different response in the simulations is due to the ionization location of the injected nitrogen. Low electron temperatures in the private flux region (PFR) in L-mode

---

[a] Invited paper, published as part of the Proceedings of the 56th Annual Meeting of the APS-DPP, New Orleans, LA, Oct 2014.

[b] Electronic mail: lorejd@ornl.gov

result in a PFR plasma that is nearly transparent to neutral nitrogen, while in H-mode the impurities are ionized in close proximity to the injection location, with this latter case yielding a largely axisymmetric radiation pattern in the scrape-off-layer. The consequences for the ITER gas injection system are discussed. Quantitative agreement with the experiment is lacking in some areas, suggesting potential areas for improving the physics model in EMC3-EIRENE.

I. Introduction

A significant challenge facing future fusion reactors is the realization of operating scenarios that can meet the limits set by the material properties of the plasma-facing components (PFCs) while simultaneously maintaining good core confinement. The heat handling capability of current divertor PFCs limits the steady-state incident power flux density to ~10 MW/m^2 [1], while at large ion fluences the stationary electron temperature at the sheath entrance must be reduced to ~5 eV or less to reduce the physical sputtering yield to acceptable levels [2]. Operation with partial detachment of the divertor offers a promising solution to these issues, and is envisioned as an operating scenario for ITER equipped with a tungsten divertor [1] using extrinsic impurity seeding (e.g., N_2, Ne, Ar) to maintain the required level of boundary radiation. The impurity will be injected through a set of toroidally distributed localized gas valves situated below the divertor cassettes [3]. Spatial localization of the impurity source, particularly under failure scenarios, may result in toroidal asymmetries in the radiated power, and possibly the heat flux to the divertor, made worse if the extrinsic gas is only partially recycling (e.g., N_2).

To investigate this potential for asymmetry and benchmark numerical modeling tools to be used for ITER predictions, a series of dedicated experiments were performed on the Alcator C-Mod tokamak [4], which is equipped with a gas injection system with the flexibility to produce varying levels of toroidal localization, and can produce ITER-relevant divertor densities at high magnetic field strength. Initial Ohmically heated L-mode experiments showed a significant level of toroidal asymmetry in several

divertor diagnostics with one divertor gas injector active [5]. In particular, reproducable asymmetry was measured in a primary radiating nitrogen charge state (N V) and in the divertor electron pressure near the outer strike point, with the latter implying asymmetry in the divertor heat flux. Numerical modeling of these experiments was performed using the 3D plasma and kinetic neutral particle transport code EMC3-EIRENE [6,7], which showed that the asymmetries could be qualitatively explained due to toroidally localized ionization of the injected nitrogen in the scrape-off-layer (SOL) near the outer strike point [8]. In the simulations, the neutral nitrogen penetrates into the SOL due to the low electron temperature (T_e) and density (n_e) in the private flux region (PFR). A significant fraction of the newly ionized nitrogen ions reach the divertor in the parallel direction before they complete one toroidal transit, resulting in toroidal asymmetry in the impurity radiation and the divertor electron pressure. Comparison with the experimental results showed good qualitative agreement in the toroidal trends in the electron pressure and N V emission in the SOL. However quantitative discrepancies were identified in the PFR, with the simulations typically resulting in colder, denser divertor conditions than are measured in experiment (see Ref. [9] for a description of a similar discrepancy in 2D fluid modeling).

In order to investigate the impact of localized impurity injection under plasma conditions more relevant to ITER [10], similar experiments were performed using high-power Enhanced D-alpha (EDA) [11] H-mode plasmas where the gas puff was used to partially detach the divertor. In these experiments, discussed in detail below, a single toroidally localized gas puff was sufficient to detach the divertor plasma and resulted in a small toroidal asymmetry in the divertor heat flux and electron temperature. As for the previous L-mode case study, 3D modeling has been used both to understand the differences between the L- and H-mode results, and to progress towards validated codes that can make reliable predictions for future devices. This paper presents the result of the H-mode localized impurity injection experiments, and describes their simulation using EMC3-EIRENE. Where appropriate, potential areas for advancing the physics model in the code to improve quantitative agreement will be identified.

II. Experimental results

Alcator C-Mod is equipped with a set of five gas injection capillaries located in the so-called divertor slot, spaced equally around the torus (see Fig. 1). This gas system has a similar layout to the six gas injectors planned for ITER [3]. At the time of writing, the ITER organization has not yet decided if the six injection points will be used simply as single entry points for the gas, or if each point will branch into a toroidally extended ring. The results described here will help guide this decision. The C-Mod experiments were performed with deuterium main ion plasmas with plasma current I_p=0.8 MA, toroidal field strength B_t=5.4 T (∇B drift direction towards the X-point), edge safety factor q95=4.6, core electron density n_e~$2.5\cdot10^{20}$ m^{-3}, input power P_{in}=3.5-4.0 MW, and the power radiated inside the separatrix $P_{rad\text{-}core}$~0.5-1 MW. The equilibrium was lower single null, with an outboard midplane radial separation of the inner and outer separatrices (dr_{sep}) of ~6mm, which places the gas capillary in the PFR, ~8 cm below the outer strike point (OSP) as shown in Fig. 1b. In these plasmas, both the plasma current and toroidal field directions are oriented clockwise when viewed from the top of the torus.

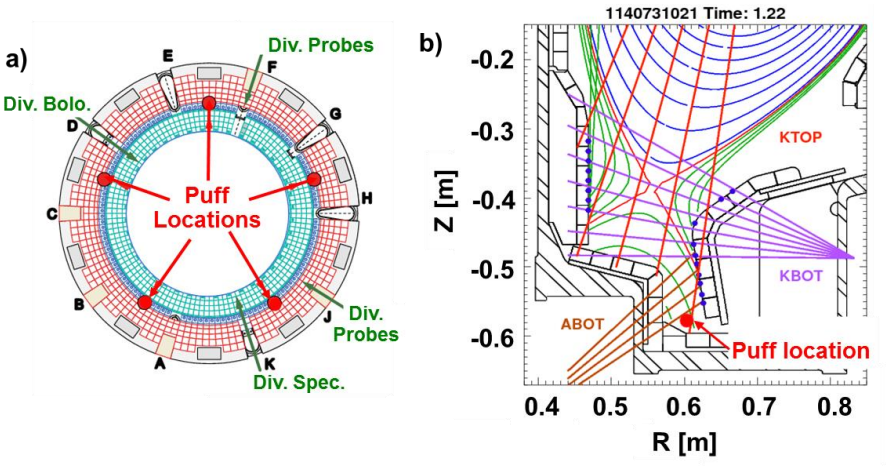

Figure 1. Location of gas injection capillaries and divertor diagnostics in Alcator C-Mod a) overhead view and b) poloidal cross section, showing also the magnetic equilibrium reconstruction of a typical discharge used in the experiments described here.

The experiments were set up in a similar fashion as those described in Ref. 10, in which main chamber impurity seeding from the outboard midplane was used to partially detach the divertor plasma. Figure 2 (black traces) shows the time history of a discharge where the power to the outer divertor (P_{div}^{outer}) and the outer divertor electron temperature ($T_{e,div}^{outer}$), measured by Langmuir probes and an infrared camera, respectively. Both P_{div}^{outer} and $T_{e,div}^{outer}$ drop substantially using the divertor capillary system with all five valves active (total gas peak flow rate of 30 Torr-L/s) compared to the main chamber seeded experiment (green lines). In the divertor capillary experiments the gas reaches the plasma at t≈1s, while the main chamber seeded discharges have the N_2 injected from t≈0.5s, just before the transition to H-mode. It is seen that for similar plasmas, either injection method can lead to the same divertor conditions, with P_{div}^{outer} strongly reduced and $T_{e,div}^{outer}$ ~5eV while good core confinement is maintained (H-factor and pedestal temperature unaffected). For a similar $P_{SOL} = P_{tot} - P_{rad,core} \approx$ 2 MW, the capillary seeded discharges also have a reduced Z_{ave}, here given by the line-averaged Z_{eff} from a toroidally viewing visible bremsstrahlung diagnostic.

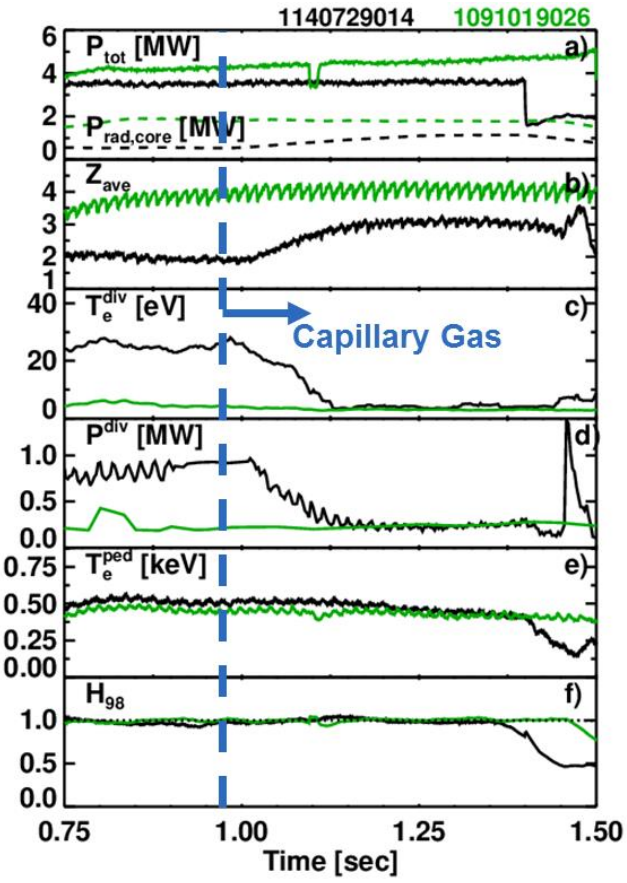

Figure 2. Comparison of divertor (black) and main chamber (green) seeded discharges, a) Total (solid) and core radiated (dashed) power, b) average Z, c) divertor T_e, d) power to the outer divertor, e) pedestal T_e, and f) H-factor.

In order to determine if localized impurity sourcing results in toroidal asymmetries in the main plasma and impurity ion conditions, the gas injectors were sequentially activated in separate (otherwise similar) discharges. By comparing the toroidally fixed diagnostic data relative to the toroidal position of the active puff, it was also determined that the divertor could be detached using a single injector with minimal toroidal asymmetry in the main plasma conditions. Figure 3 shows results from three discharges with similar levels of gas input (peak flow rate ~22 Torr-L/s). In each case $T_{e,div}^{outer}$ drops to ~5 eV, while P_{div}^{outer} is strongly reduced. Figure 4 shows divertor T_e and parallel heat flux profiles from the gas location

scan (colors correspond to the active puff location). The electron temperature from a single probe is plotted versus toroidal angle of the puff (angle increasing when viewing the torus from above) relative to the diagnostic in Fig. 5a. It can be seen that any toroidal trends in the main plasma conditions are small compared to the shot-to-shot variation, in contrast to the L-mode results (cf. Fig. 5 in Ref. 8).

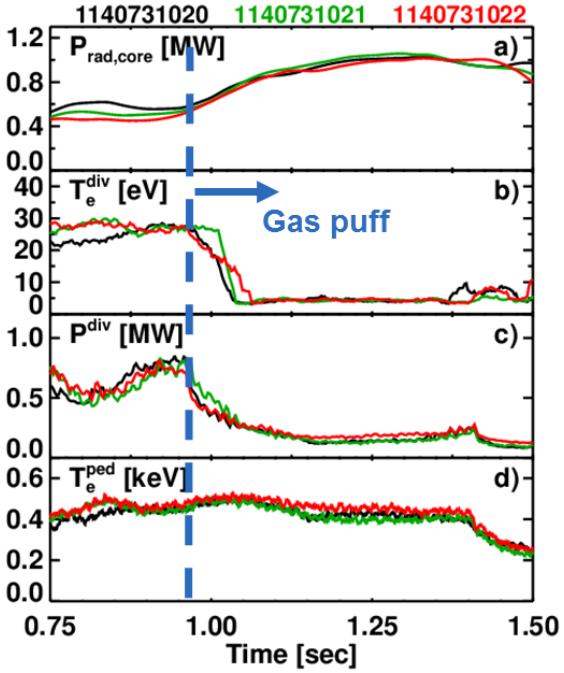

Figure 3. a) Core radiated power, b) divertor T_e, c) power to the outer divertor, and d) pedestal T_e for three different divertor gas capillaries.

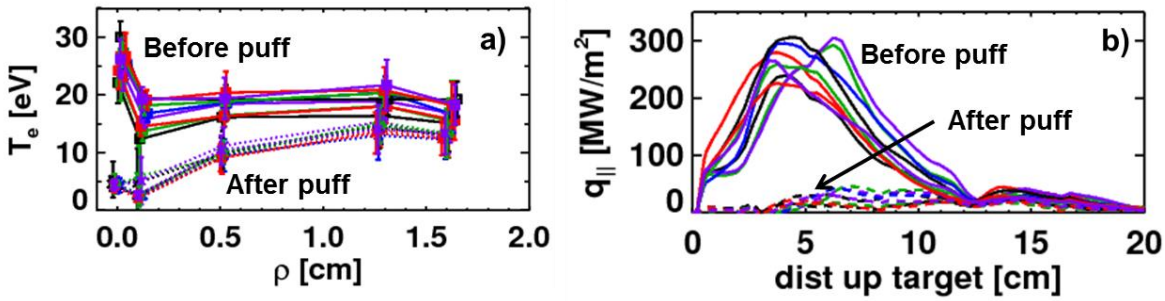

Figure 4. a) Electron temperature profiles and b) parallel heat flux profiles on the outer divertor before (solid lines) and after the gas puff (dashed lines). Colors correspond to different gas injection locations, see Fig. 5.

On the other hand, clear toroidal asymmetry was measured in the nitrogen emission in the PFR. Fig. 5b shows the toroidal variation in the N II emission (λ=399.50 nm) from a view observing the outer strike point from the top of the device. It was found that the asymmetry decreased with increasing charge state, with the strongest variation found in the N II emission, a weaker trend in N III (λ=437.99 nm), and no toroidal asymmetry observed in N IV (λ=405.78 nm). This is in contrast to the L-mode results, which showed strong asymmetry in both VUV and visible N V emission.

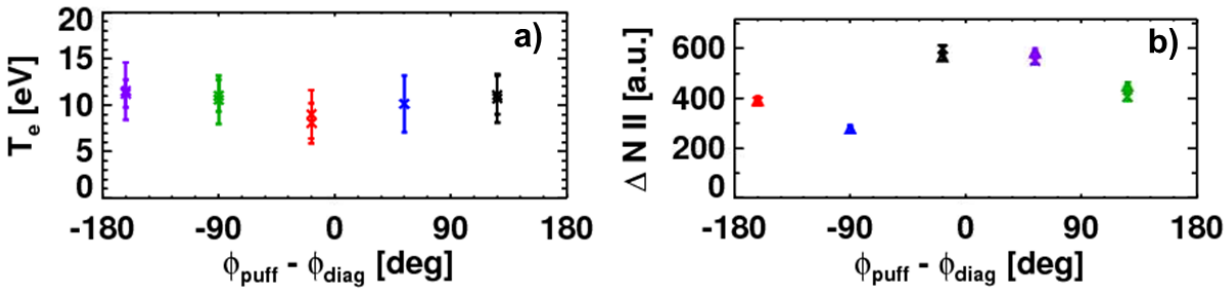

Figure 5. Toroidal variation in the a) divertor T_e and b) N II emission as a function of the toroidal angle relative to the active puff location.

Although the divertor could be partially detached with either one or five injection locations, it was found that the compatibility with good core confinement had a nonlinear dependence on the amount of gas injected and the number of injection locations. Figure 6 shows time history of three discharges with similar total gas flow rates (32-38 Torr-L/s) through five (black), two (green) and one (red) capillary. While in each case the P_{div}^{outer} and $T_{e,div}^{outer}$ are strongly reduced, the two and single capillary cases show a degradation in the H-factor and drop in the pedestal temperature shortly before the plasma fully detaches and the radiation structure shifts to become localized to the x-point. Partial detachment with

high confinement using a single capillary ultimately required ~60% of the total peak gas flow rate as compared to when all five valves were active.

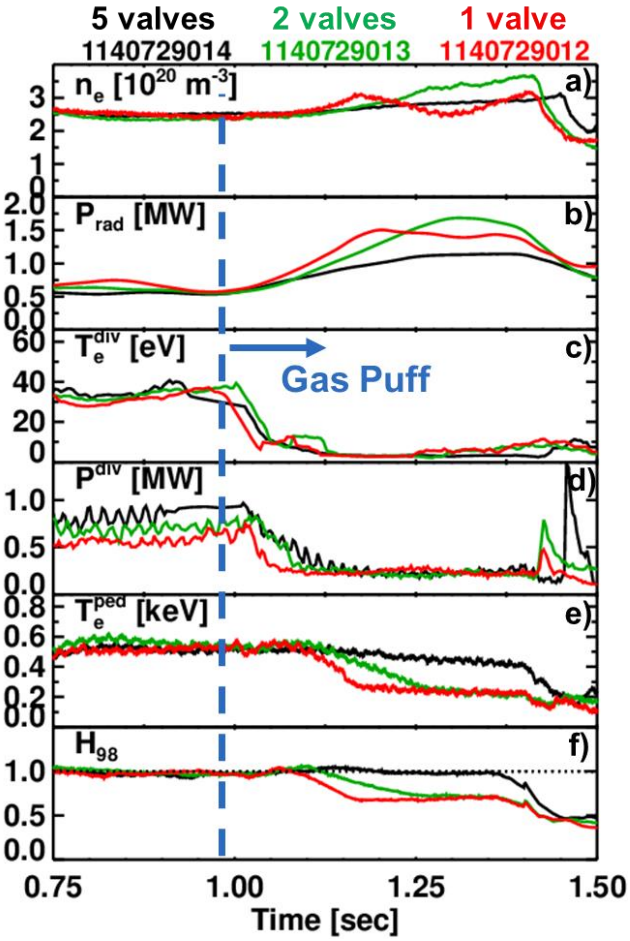

Figure 6. a) Comparison of discharges with 5 (black), 2 (green), and 1 (red) active divertor capillaries, a) line averaged density b) core radiated power, c) divertor T_e, d) power to the outer divertor, e) pedestal T_e, and f) H-factor.

III. EMC3-EIRENE simulations

The EMC3-EIRENE code package, originally developed for stellarator systems, has now been applied to a wide variety of plasma experiments [12]. EMC3 solves the 3D fluid transport equations (continuity, parallel momentum, ion and electron energy) for an arbitrary magnetic field with classical parallel

transport and diffusive cross-field transport with manually specified diffusivities. EMC3 is coupled to the 3D kinetic neutral particle transport and plasma surface interaction code EIRENE, which provides the particle, momentum and energy sources and sinks due to plasma-neutral interactions in a given plasma background. The two codes are iterated until the results reach an acceptable convergence (typically 1-2% change in the downstream plasma conditions). EMC3 also includes a trace impurity neutral and ion transport model that includes feedback to the main plasma through an electron cooling term. While EMC3 allows for the simulation of plasma fluid transport in three dimensions, it has several limitations, particularly in comparison with advanced 2D fluid transport codes such as SOLPS [13]. For example, the version used here does not include cross-field drifts, kinetic corrections in the form of flux limiters, or volume recombination.

During a typical simulation, the computational grid, aligned in the toroidal direction to the magnetic field, and the PFCs intersecting the grid are specified. For the simulations presented here, the magnetic field is calculated by EFIT [14] and the PFCs are taken to be axisymmetric. The computational grid used is similar to that shown in Ref. 8, however due to the small dr_{sep} in these experiments a disconnected double-null grid [15] was developed for Alcator C-Mod. To simulate the effect of a single injection location, the grid spans the entire toroidal extent, consisting of ~8 million cells. Due to the large grid size and the correspondingly large number of Monte-Carlo particles required, each simulation requires approximately 2-3 weeks of wall clock time on a system with ~30 2 GHz processors. The density on and the input power across the core boundary are taken from experimental conditions, and the cross-field diffusivities are scaled to approximately match the upstream profiles from Thomson scattering as shown in Figure 7. Atomic nitrogen is injected into the divertor slot with a recycling (self-sputtering) coefficient of 0.5.

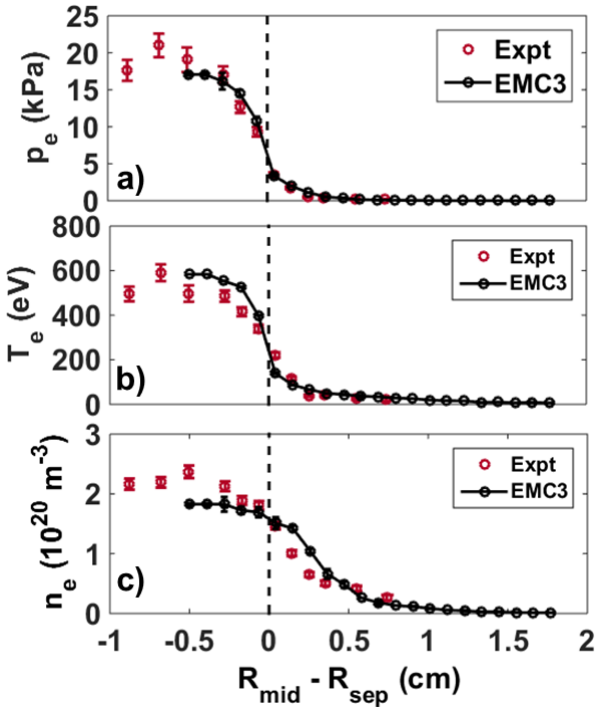

Figure 7. Upstream electron a) pressure, b) temperature, and c) density from Thomson scattering (red) and EMC3-EIRENE simulations (black).

In similar simulations of Ohmically heated L-mode plasmas [8], it was found that the low electron temperature in the PFR resulted in a plasma that was nearly transparent to the injected neutral nitrogen. As a result, nearly all of the nitrogen ionization occurred above the separatrix legs in the SOL. The H-mode simulations have exactly the opposite trend. Due to the higher T_e and n_e (resulting from the higher P_{SOL}), the ionization mean-free-path is very short in the PFR, as shown in Fig. 8. As a result, the seeded nitrogen is ionized in close proximity to the injection location, and nearly all of the initial ionization is in the PFR. In order for the nitrogen to reach the common flux region of the SOL, and radiate power in the flux tubes carrying heat to the divertor, the impurities must be transported via slow cross-field diffusion. This results in a radiated power distribution that is largely axisymmetric, with low toroidal asymmetry in the downstream plasma conditions. An example is shown in Fig. 9, illustrating

that $T_{e,div}^{outer}$ has a small toroidal variation, on the order of the experimental uncertainty in the single puff scan.

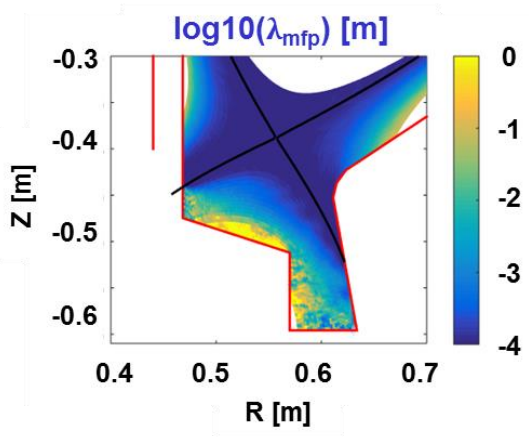

Figure 8. Atomic nitrogen ionization mean-free-path calculated from the EMC3-EIRENE simulated electron temperature and density.

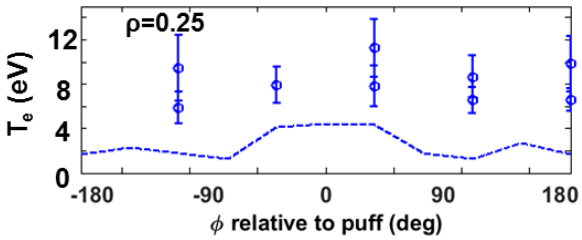

Figure 9. Divertor electron temperature as a function of toroidal angle relative to the puff location from experiment (circles with error bars) and from EMC3-EIRENE (dashed line).

Another effect acts to reduce the toroidal asymmetry in the simulations. Since the impurities are ionized near the puff location, they stream freely as ions along the field lines until their intersection with the PFCs. Figure 10 shows the intersection of a field line initiated at the puff location, 90 degrees away. At this intersection, 50% of the incident ions are re-emitted as neutral nitrogen atoms, resulting in a cloud of recycled neutral nitrogen gas. This essentially acts as a second neutral nitrogen source in the PFR. The

net result is that ionization of the seeded impurities in the PFR results in a small toroidal asymmetry in the main plasma conditions, and thus the heat flux, in the simulations. This is in contrast to the L-mode simulations, which showed that ionization in the SOL resulted in a strong toroidal asymmetry.

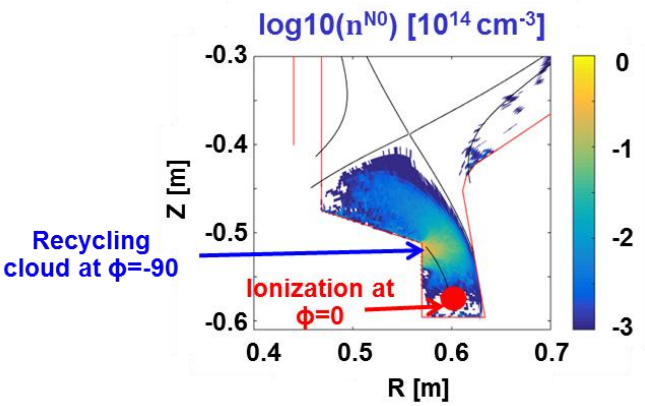

Figure 10. Recycling of the ionized injected nitrogen where the flux tubes initiated from the puff location intersect the PFCs, 90 degrees away from the puff.

While the simulations provide a qualitative mechanism that explains the different levels of toroidal asymmetry measured in the main plasma conditions at the divertor in L- and H-mode, there are several important quantitative differences between the simulated and measured data. The simulations with a single puff location were unable to reproduce an electron temperature reduction across the entire outer target, as seen experimentally in Fig. 4a. As shown in Fig. 11, T_e is reduced as compared to the pre-puff value within a few millimeters of the outer strike point. However the post-puff temperatures are larger than the experimental values at $0.5<\rho<1$cm. Increasing the amount of nitrogen injected in the simulation extended the radial extent of the temperature drop slightly, however a significant increase in the gas input caused an unstable progression of the detachment front towards the x-point, and numerical instability in the simulation, similar to the movement of the radiation front towards the x-point seen in the discharges with increased nitrogen influx. It is possible that the addition of physics missing in the current code version, such as volume recombination and kinetic corrections, could

improve the quantitative agreement in the main plasma parameters in this region. On the other hand, the divertor electron temperature profiles could be approximately reproduced with multiple puff locations in the simulation, as shown in Fig. 11. In this case the electron temperature is reduced from 0<ρ<1cm, as in the experiment, and the heat flux is suppressed across the outer target (Fig. 11c). Future modeling may determine if the threshold behavior in the detachment level and its dependence on the number of gas locations and the amount of nitrogen injected is related to the similar behavior observed in the experiment, as discussed in section II.

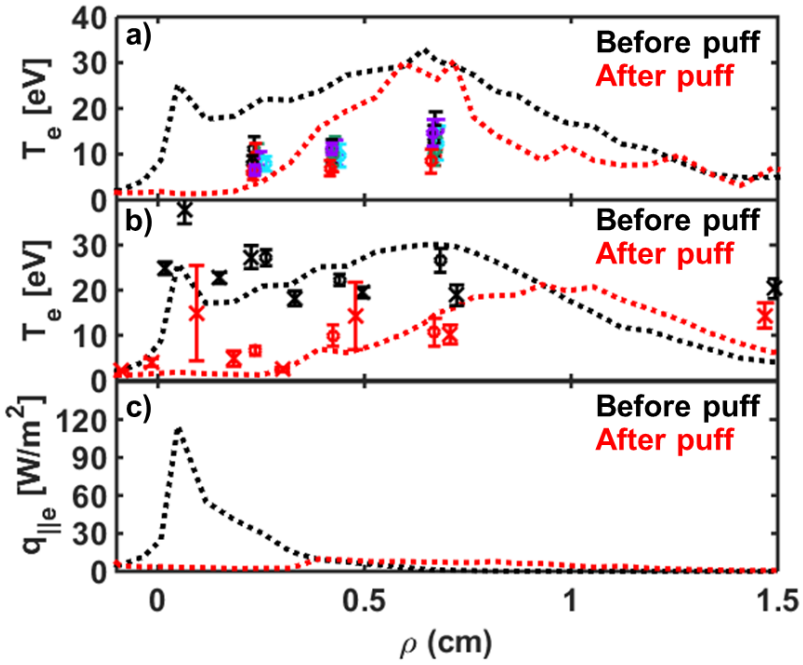

Figure 11. a) Divertor T_e calculated by EMC3-EIRENE before (black dashed line) and after (red dashed) a single puff is applied and probe measurements after the puff (symbols, colors correspond to puff location). b) Divertor T_e and c) $q_{||e}$ calculated by EMC3-EIRENE (dashed lines) and measured by probes (symbols) before (black) and after (red) nitrogen is puffed simultaneously from 5 puff locations.

The simulations do show toroidal asymmetries in the nitrogen emission in the PFR however, as shown in the L-mode analogue to this work [8], the qualitative comparisons are poor in this region. It is highly

likely that cross-field drifts, shown to be experimentally important in the PFR [16,17,18] will be required to match the experimental trends in the PFR conditions. Drifts will also affect the heat transport into the PFR, which is assumed to be purely diffusive with the diffusivities scaled to match the upstream conditions. Since the results presented are dependent on the PFR conditions, future modeling with improved physics detailing a comparison of main and impurity plasma parameters in the PFR is required to test the robustness of the mechanisms described.

IV. Summary

Previous experiments performed on Alcator C-Mod with localized nitrogen impurity injection in the PFR showed strong, repeatable toroidal asymmetries in the downstream main plasma conditions in L-mode. New experiments exploring the level of asymmetry in high-power, EDA H-mode plasmas showed the non-axisymmetry in divertor conditions seen in L-mode to be strongly reduced. The divertor plasma could be partially detached without significant degradation in the core confinement using five poloidally and toroidally localized divertor gas injectors, or only a single injector. However, the gas flow rate had to be tailored in each case, as injecting too much gas through a small number of valves resulted in degraded pedestal and core confinement. These results suggest that toroidal asymmetries introduced by toroidally distributed gas injectors may not be an issue for ITER, and the system may be robust to a valve failure if the gas flow rate can be carefully controlled and indicators of radiation instabilities, such as a shift of the radiation front towards the x-point, can be monitored. Additional work is required to understand the relationship between the number of injection locations and the gas flow rate threshold that results in degraded core confinement. This should also include any impact that ELM mitigation strategies may have, such as the use of rotating or stationary non-axisymmetric magnetic fields, which may interact with localized impurity seeding.

Earlier simulations performed using the 3D edge transport code EMC3-EIRENE showed that the strong asymmetry in L-mode could be qualitatively explained by the penetration of the injected neutral nitrogen into the SOL, while the ionization of the nitrogen in the PFR due to the higher electron density and temperature in H-mode results in mostly axisymmetric main SOL plasma conditions. Quantitative matching of the experimental conditions remains challenging, as well as qualitative agreement of the impurity emission trends in the PFR. Additional physics missing in the current version of the code, such as cross-field drifts, volume recombination, and flux limiters may improve this comparison, although the latter is not expected to have a large effect for the high collisionality of the H-mode divertor plasmas studied here. Implementation of volume recombination into the code is under active development. Experiments and simulations run with an injected impurity such as neon may help elucidate the underlying physics by changing the recycling coefficient (and thus the impurity source distribution), radiation patterns, and recombination mechanisms.

V. Acknowledgement

This work is supported by D.O.E. contracts DE-AC05-00OR22725 and DE-FC02-99ER54512. The views and opinions expressed herein do not necessarily reflect those of the ITER Organization.

[1] R.A. Pitts, S. Carpentier, F. Escourbiac, T. Hirai, V. Komarov, S. Lisgo, A.S. Kukushkin, A. Loarte, M. Merola, A. Sashala Naik, R. Mitteau, M. Sugihara, B. Bazylev, P.C. Stangeby, J. Nucl. Mater. 438 (2013) S48.

[2] P.C. Stangeby and A.W. Leonard, Nucl. Fusion 51 (2011) 063001.

[3] S. Maruyama, Y. Yang, G. Kiss, M. O'Connor, M. Sugihara, P. Sergei, S. Michiya, R. Pitts, L. Bo, L. Wei, Y. Pan, M. Wang, L. Baylor, S. Meitner and D. Douai, IAEA FEC, San Diego 2012, paper ITR/P5-24.

[4] E.S. Marmar and the Alcator C-Mod Group, Fusion Sci. Technol. 51 (2007) 261.

[5] M.L. Reinke, B. Lipschultz, B. LaBombard, R.M. Churchill, J. Lore, J. Canik, R. Pitts, PSFC Research Report PSFC/RR-14-3, MIT, Cambridge (2014).

[6] Y. Feng, F. Sardei, J. Kisslinger and P. Grigull, J. Nucl. Mater., 241 (1997) 930.

[7] Y. Feng, F. Sardei and J. Kisslinger, J. Nucl. Mater. 266 (1999) 812.

[8] J.D. Lore, M.L. Reinke, B. LaBombard, B. Lipschultz, R.M. Churchill, R.A. Pitts and Y. Feng, Journ. Nucl. Mater., "EMC3-EIRENE modeling of toroidally-localized divertor gas injection experiments on Alcator C-Mod", (2014) DOI: 10.1016/j.jnucmat.2014.09.053.

[9] A.V. Chankin, D.P. Coster, R. Dux, Ch. Fuchs, G. Haas, A. Herrmann, L.D. Horton, A. Kallenbach, B. Kurzan, H.W. Mueller, R. Pugno, M. Wischmeier, E. Wolfrum and the ASDEX Upgrade Team, Nucl. Fusion 49 (2009) 015004.

[10] A. Loarte, J.W. Hughes, M.L. Reinke, J.L. Terry, B. LaBombard, D. Brunner, M. Greenwald, B. Lipschultz, Y. Ma, S. Wukitch and S. Wolfe, Phys. Plasmas **18**, 056105 (2011).

[11] M. Greenwald, R. L. Boivin, F. Bombarda, P. T. Bonoli, C. L. Fiore, D. Garnier, J. A. Goetz, S. N. Golovato, M. A. Graf, R. S. Granetz, S. Horne, A. Hubbard, I. H. Hutchinson, J. H. Irby, B. LaBombard, B. Lipschultz, E. S. Marmar, M. J. May, G. M. McCracken, P. O'Shea, J. E. Rice, J. Schachter, J. A. Snipes, P. C. Stek, Y. Takase, J. L. Terry, Y. Wang, R. Watterson, B. Welch, and S. M. Wolfe, Nucl. Fusion 37, 793 (1997).

[12] Y. Feng, H. Frerichs, M. Kobayashi, A. Bader, F. Effenberg, D. Harting, H. Hoelbe, J. Huang, G. Kawamura, J.D. Lore, T. Lunt, D. Reiter, O. Schmitz and D. Sharma, Contrib. Plasma Phys. **54** (2014) 426.

[13] Schneider R., Reiter D., Zehrfeld H.P., Braams B., Baelmans M., Geiger J., Kastelewicz H., Neuhauser J. and Wunderlich R. 1992 J. Nucl. Mater. 196–198 810.

[14] L.L. Lao, H. St. John, R.D. Stambaugh, A.G. Kellman and W. Pfeiffer, Nucl. Fusion 25 (1985) 1611.

[15] J.D. Lore, J.M. Canik, Y. Feng, J.-W. Ahn, R. Maingi and V. Soukhanovskii, Nucl. Fusion **52** (2012) 054012.

[16] N. Smick, B. LaBombard, and I.H. Hutchinson, Nucl. Fusion **53** (2013) 023001.

[17] C.J. Boswell, J.L. Terry, B. LaBombard, B. Lipschultz, J.A. Goetz, J. Nucl. Mater **290-293** (2001) 556.

[18] J.A. Boedo, M.J. Schaffer, R. Maingi, C.J. Lasnier, Phys. Plasmas **7** (2000) 1075